

Slope Stability and Pore-Water Pressure Regime in Response to Rainfall: a Case Study of Granitic Fill Slope in Northern Thailand

A. Jotisankasa¹, K. Mahannopkul² and A. Sawangsuriya³

¹Department of Civil Engineering, Kasetsart University, Bangkok, Thailand

²Department of Civil Engineering, Kasetsart University, Bangkok, Thailand

³Bureau of Road Research and Development, Department of Highways, Bangkok, Thailand

E-mail: fengatj@ku.ac.th

ABSTRACT: Spatial and temporal variations of pore water pressure within slopes in response to rainfall that lead to slope failure, are one of the major uncertainties in evaluating slope stability. This paper reports on the study of slope stability with respect to pore water pressure variation with rainfall during actual failure in September 2011. The studied slope, situated near the peak of Doi-Inthanon national park, Northern Thailand, consisted of granitic residual soil fill that suffered from soil erosion and shallow failure. The KU-tensimeters were installed to monitor both pore water pressure and suction in the slope. Various laboratory and field tests were conducted, namely, direct shear tests on both fully saturated and unsaturated soils, soil water characteristic curve, and field infiltration tests. Two-dimensional (2-D) Back analysis of slope stability, for failure event in 2011 suggested that the critical pore water pressure distribution can be assigned to the r_u value of about 0.43 or $u=0.43\gamma H$. Based on three dimensional (3-D) stability analysis, the pore water pressure can be 30% higher when compared with the 2-D analysis. 2-D Finite Element seepage analysis appeared to capture general trend of pore-water pressure change reasonably well. However, it seemed to underpredict the pore-water pressure at failure especially for depth greater than 2 meters.

Keywords: Slope stability, Pore-water pressure, Rainfall, Suction, Granitic soil.

1. INTRODUCTION

Rainfall-induced landslides have increasingly posed serious threats to infrastructure and people's lives around the world. This problem is expected to be even more serious in near future due to climate change which would result in more intense rainfall, longer drought period and possible subsequent change in vegetation cover. In order to mitigate such geo-hazard, e.g. by means of slope stabilization or early warning system, an in-depth understanding of the interaction between climate and slope stability is required.

Generally, rainfall event brings about reduction in soil suction and increase in positive pore-water pressure from several sources, such as direct rainwater infiltration into slope, subsurface seepage through stratified soil layers and spring from bedrock (Johnson & Sitar, 1990) as well as influx of surface runoff into slope from surrounding area. Shear strength of the slope material is subsequently reduced by such pore water pressure increase until a critical point is reached when significant slope movement commenced. Flow-type landslide has also been shown to be triggered by static liquefaction, i.e. the excess pore-water pressure induced by undrained shearing, in particular, of loose materials (e.g. Wang et al., 2002, Olivares & Picarelli, 2003, Chen et al., 2004, Cascini et al., 2010, Buscarnera & di Prisco, 2012)

The interaction between rainfall and pore-water pressure regime in slope is very complex, depending on many factors, such as soil type, climate, topography, geology as well as vegetation. Consequently, a number of studies have been directed at monitoring field performance of slope in order to gain to better understanding of pore water pressure and suction changes in relation with rainfall (e.g. Tsaparas et al., 2003, Ng et al., 2003, Sorbino & Nicotera, 2013). Nevertheless, rarely reported in the literature is the variation of pore water pressure monitored during the time of actual slope failure. Spatial and temporal variations of pore water pressure within slopes in response to rainfall still remain the major uncertainties in evaluating slope stability.

This paper presents the extensive field monitoring results of pore-water pressure and rainfall of a granitic soil slope near the peak of Doi-Inthanon national park, Northern Thailand. The study also involved laboratory determination of the saturated-unsaturated shear strength and Soil-Water Characteristic Curves (SWCC). In particular, back analysis of the soil slope which failed in 2011 was performed in order to determine the critical pore-water pressure at

failure based on laboratory shear strength. Seepage analysis was also performed in order to reproduce the pore water pressure variation with rainwater infiltration with an aim of linking climate with slope stability.

2. DESCRIPTION OF STUDIED SITE AND INSTRUMENTS

2.1 Studied site

The studied site is a fill side-slope of highway No.1009 located from km.41+945 to km.42+715 in Doi-Inthanon National Park, Chiangmai province, Northern Thailand, as shown in Figure 1. At the elevation of 2,175m above Mean Sea Level, the climate of this site is cloud forest type with high relative humidity of air and large amount of precipitation, as shown in Figure 2. The total number of rainy days in Year 2011 was 192 days with total annual rain of 3,462 mm. This results in high soil moisture and pore-water pressure in the ground and consequently soil erosion is not uncommon in the area.



Figure 1 Map and aerial photos of the studied site

The studied slope had previously suffered from severe erosion and shallow slope failure due to heavy rainfall event in 2009, after which an extensive stabilization scheme was implemented. The site was divided into five plots (A, B, C, D and E in Figure 1), each of which involved different five erosion control technique as well as horizontal drains (Sawangsurriya et al., 2013, Jotisankasa et al., 2014). Based on field observation in 2011, erosion control performance of these five sections was then compared. It was suggested that erosion control at Plot A, which consisted of erosion control blanket/logs, and clay sodding appeared to be the most effective, given the conditions of accumulated rainfall less than 1,400 mm/year and 4-day accumulated rain of less than 200 mm. However, in September 2011, as the accumulated rainfall was over 3,400 mm/year and 4-day accumulated rain exceed 200 mm, all test sections suffered from severe shallow slope failure and surface erosion. In particular, Plot A suffered from shallow slope failure as shown in Figure 3. The daily rainfall during slope failure was plotted against corresponding 3-day antecedent rainfall as shown in Figure 4. This sort of rain patterns and critical rainfall envelope provide a useful tool for roughly estimating when slope failure is likely to occur, as suggested by many previous researchers (e.g., Lumb, 1975, Crozier & Eyles, 1980, Mairaing et al., 2012).

Owing to the better completeness of field monitoring data at Plot A and its relatively better performance, only Plot A slope will be described in this paper. Figure 5 shows the cross-section of Plot A, including estimated slip surface of failure that took place in September 2011.

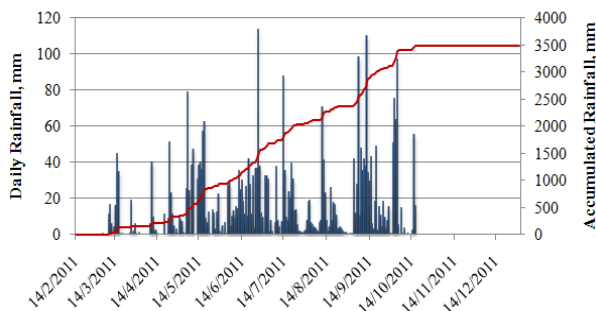


Figure 2 Variation of daily rainfall in 2011



Figure 3 Slope failure and its escarpment at Plot A

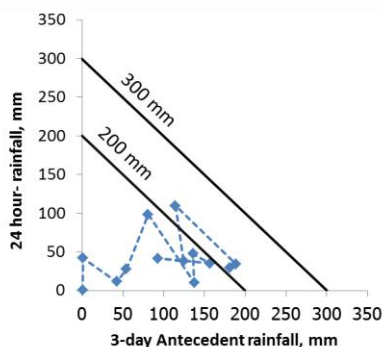


Figure 4 Rainfall pattern that triggered failure in September 2011

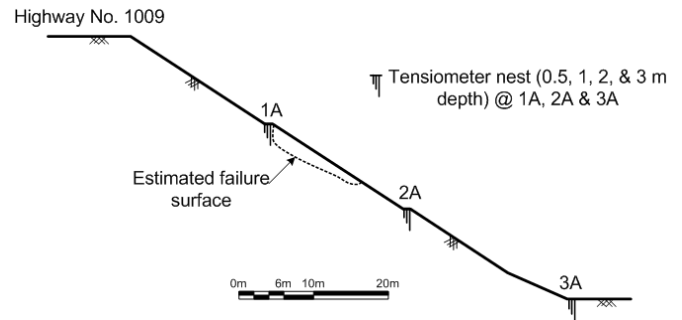


Figure 5 Sketch of studied slope, instruments and location of failure surface

2.2 Ground profile

Ground profile at the site was investigated by means of light weight dynamic penetrometer, so-called Kunzelstab penetration test (weight of 10kg, with falling height of 0.5 metre) as well as test pit dug into the escarpment of slope failure. The slope consists of a decomposed granitic soil fill, which comprises of rather heterogeneous alternating layers of two types of soils (i.e. reddish clayey sand, SC, and whitish silty sand, SM). Granite boulders were also sometimes found mixed with these soils. Double ring infiltration tests were performed in the test pit at three depths in order to estimate the value of saturated permeability. As shown in Figure 6, at greater depth, the soil appeared to be of smaller permeability due to the greater clay content and greater density. This trend is also in a good agreement with increasing value of Kunzelstab (KPT) blow count with depth. Table 1 summarises basic properties of the two materials at the site.

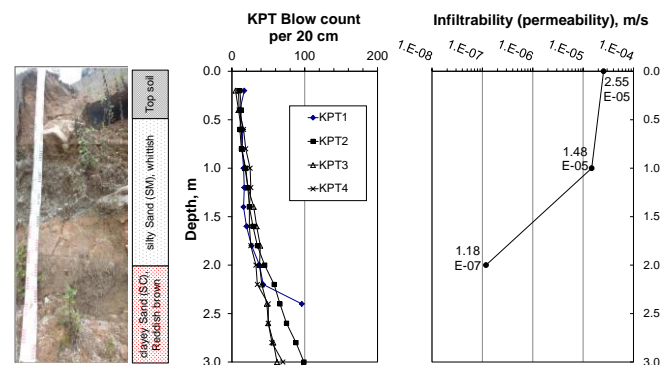


Figure 6 Soil profile and variation of permeability (infiltrability) with depth

Table 1 Basic soil properties

Soil	SC	SM
Description	Clayey sand, Reddish brown	Silty sand, Whitish
%Sand	58.7	76.9
%Silt	17.5	17.7
%Clay	22.5	3.4
Liquid Limit, %	30.2	NA
Plastic Limit, %	20.1	NA
Plasticity Index, %	10.1	NA
Void ratio	0.616	0.627

2.3 Instrumentations

Despite annual high precipitation at the site, ground water table in the slope during non-rainy season is normally at great depth and soils are unsaturated with suction or negative pore-water pressure in those few dry months. Consequently, the device used for monitoring the pore water pressure in the studied slope was required to be capable of monitoring both positive pressure and negative pressure or tension. At Kasetsart University (KU), Jotisankasa et al., (2007) developed the KU tensiometers using MEMs pressure sensors, as shown in Figure 7. The device is able to measure pore water pressure in the range of -100 to 600 kPa, both in conventional laboratory tests (Jotisankasa & Mairaing, 2010) and in the field (Jotisankasa et al., 2010a). The KU-tensiometers were installed at three locations along the slope (1A, 2A and 3A) as shown in Figure 5. At each location, four tensiometers were installed at the depth of 0.5, 1, 2 and 3 meters.

Figure 7 shows the installation procedure of KU tensiometers in the field. Firstly, a hole was created by rotary drilling to the required depth, and afterwards a PVC tube was inserted down the hole. Any void surrounding the tube was backfilled with excavated soil and the surface was covered with PVC lid to prevent any ingress of surface water into the hole. Tensiometer was then inserted into the hole and great care was taken to ensure good contact between the tensiometer's ceramic tip and the soil below. A thin layer of clay paste was applied at the ceramic tip for that purpose. It was also ensured that the tensiometer was well saturated with water and no air bubble was present in the reservoir to avoid erroneous measurement. The field KU-tensiometer can also be easily removed from the borehole through the PVC tube, up to the ground, for re-filling with water later.

A data logger was employed for each set of four tensiometers in order to automatically record the pore-water pressure at 15 minute interval. The tipping bucket rain gauge was also installed to continuously record rainfall with 1 minute interval at the site.

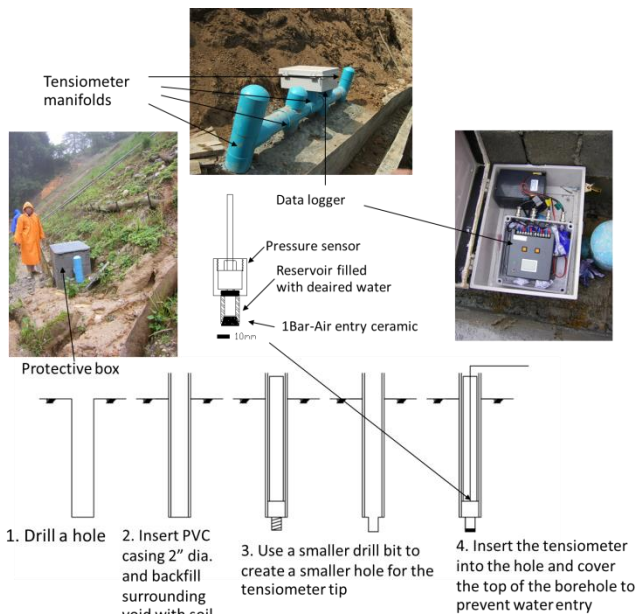


Figure 7 Tensiometer installation procedure

3. PORE WATER PRESSURE REGIME AND RAINFALL CHARACTERISTIC

Typical distributions of pore water pressure for each tensiometer nest in dry season and wet season are shown in Figure 8. Notably, during the dry season (27/2/11), suction was generally present in the slope (i.e. negative pore water pressure), while towards the end of wet season (15/9/11), rainfall infiltrated into the slope resulting in rise in perched ground water table and positive pore-water pressure.

Interestingly at Station 3A, (see Figure 8c), the pore-water pressure distributions were similar for both dry and wet season regardless of seasons. Figure 9 shows the contour of pore-water pressure for both dry and wet seasons. These contours were generated using contour software based on field measurement from tensiometers. It can be seen that in dry season, ground water had accumulated more around the toe of slope at Station 3A (see Figure 9a). Nevertheless, in rainy season (15/9/2011), as shown in Figure 9b, pore-water pressure appeared to be greater near station 1A. This zone of high pore-water pressure agrees very well with the location of slope failure as shown in Figure 5. All in all, these observations suggest that the critical zone of high seepage in slope is essentially seasonal. It is believed that geological setting plays an important role in controlling such changeable seepage regime and more detailed investigation needs to be done in the future.

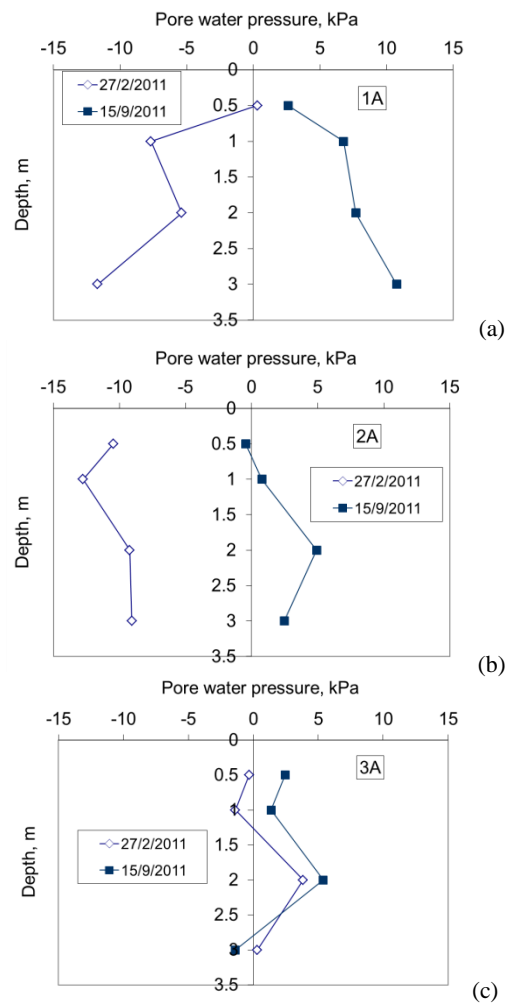


Figure 8 Comparison of pore water pressure variation with depth in dry season (27/2/2011) and rainy season (15/9/2011) at three locations 1A, 2A and 3A

In order to comprehend origins of runoff at the site, the rainfall intensities with time during failure were plotted as shown in Figure 10. Also shown was the infiltrability line, indicating saturated permeability determined from double ring infiltration test at the ground surface. Theoretically, runoff only takes place when the rainfall intensity exceeds the value of infiltrability. If considering hourly rainfall at the site as in Figure 10a, no run-off would be expected, as rainfall intensity was always less than saturated permeability. Still, when considering rainfalls of 15minute and 5 minute intervals (Figures 10b & c), only minor runoff would be expected at this site since there were only few occasions where

rainfall exceeded ground permeability. Nevertheless, since runoff had frequently been observed at the test slope, it was expected to be surface water coming from surround areas of impermeable surface (car park and road surface just above the test slope), rather than runoff from the slope area itself.

Unfortunately, due to datalogger malfunction, no results of pore-water pressure could be obtained during failure time between 3 to 14 September 2011.

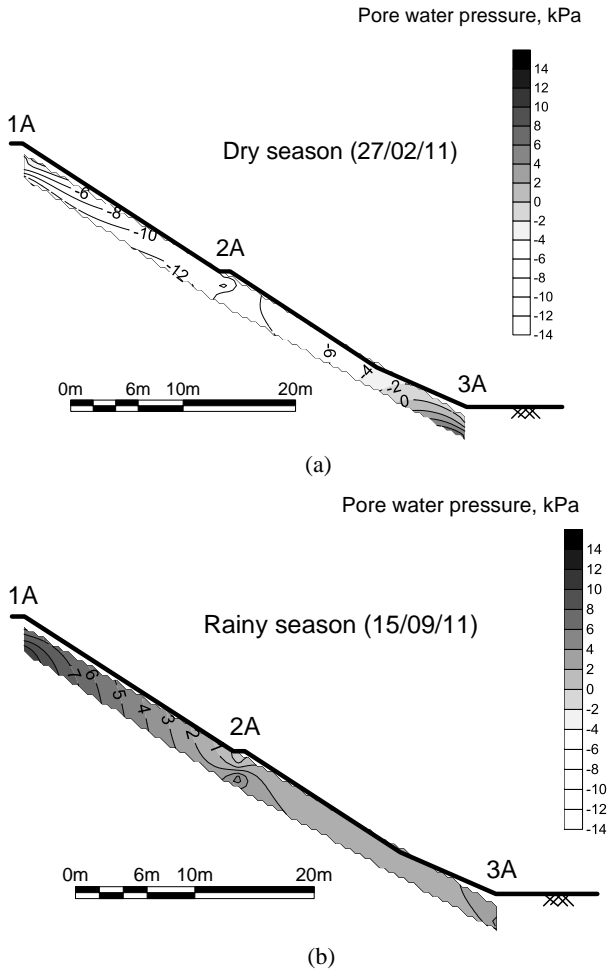


Figure 9 Contours of pore water pressure during (a) dry season, and (b) wet season

The value of hourly rainfall and corresponding 24-hour rainfall during the failure at this studied site was also compared with Hong Kong's criteria of severe landslide occurrence probability as shown in Figure 11. No such criteria are yet to exist in Thailand and therefore those of Hong Kong's (Kay, 1997) were invoked instead. It is argued that rainfalls plotted in terms of the peak-1 hour rainfall together associated 24-hour rainfall appeared to more useful than other combinations of rainfall (Kay, 1997). It is noted that Hong Kong's geology encompasses a greater variety of rocks, including volcanics, intrusives, and sedimentary rocks (Evans, 1997), while at the studied site, the rocks are mainly granitic and metamorphic.

As shown in Figure 11, interestingly, the rainfall level at the studied site would be considered as "Negligible probability of severe landslide", while in fact wide spread shallow slides and one major slide actually happened in the vicinity of the studied area. This discrepancy was thought to be partly due to the more intensive slope stabilization works that had been implemented in Hong Kong as compared to those at Doi-Inthanon National Park. This was perhaps reasonable considering a greater consequential loss of properties in Hong Kong due to landslide.

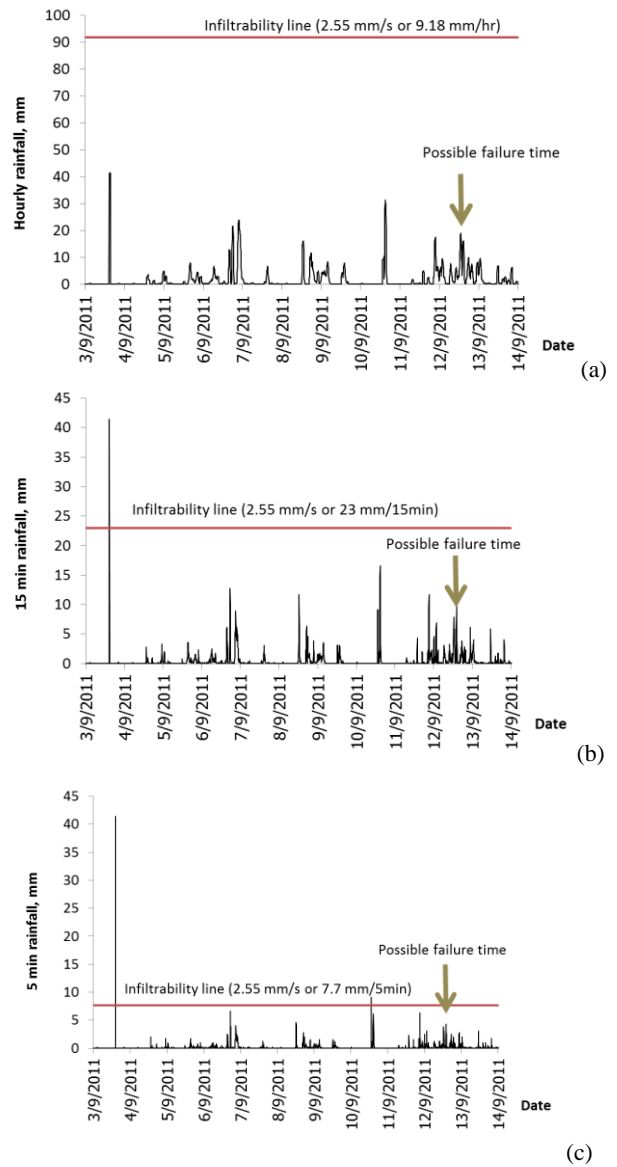


Figure 10 Variations of rainfall intensity with time (a) Hourly rainfall (b) 15min rainfall and (c) 5min rainfall

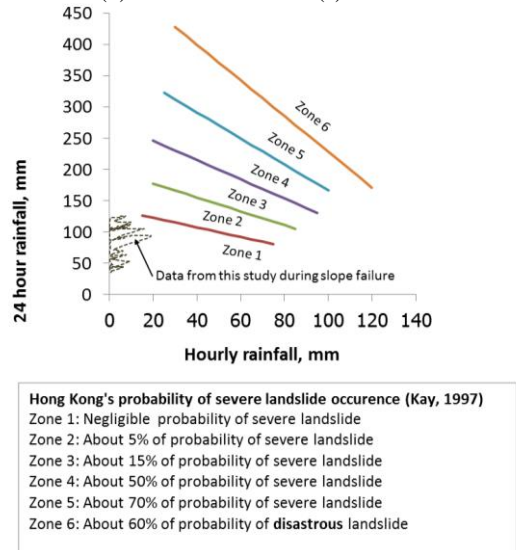


Figure 11 Comparison between rainfall data during slope failure and Kay (1997) Hong Kong's criteria

4. LABORATORY TESTS

Characteristics of the materials at the studied slope were investigated in laboratory both in saturated and unsaturated states. Intact “undisturbed” samples, collected using thin-wall miniature sampler, about 63 mm in diameter and 20 mm thickness, were tested for Soil-Water Characteristic Curve (SWCC) using the approach as explained by Jotisankasa et al. (2010b). SWCC is the relationship between suction and soil moisture content, which is required as key properties for soil-atmosphere interaction analysis of slope, such as infiltration, and for prediction of unsaturated shear strength and permeability function (Fredlund & Rahardjo, 1993)

In this study, SWCC is determined using miniature KU tensiometer (for suction less than 100 kPa) and relative humidity sensor (for suction greater than 1000 kPa). The method involved gradually wetting or drying soil sample, and during each stage suction of sample was monitored until equilibrium was reached. A minimum curing period of about 2-3 days between each increment was allowed for equilibration of the suction throughout the sample, which was carefully wrapped to prevent evaporation. Figure 12 shows the SWCCs of both soils (SC and SM) for drying and wetting paths. Notably, SC soil appeared to be able to absorb more moisture considerably more than the SM soil, for suction higher than 10 kPa, due to the higher clay content of SC soil. Hysteresis in SWCC of SC soil was also expectedly greater than SM.

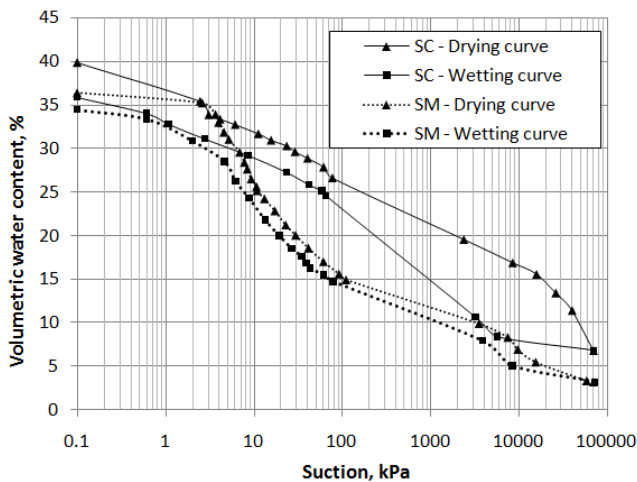


Figure 12 Soil-water characteristic curves

Shear strength characteristic of the materials at the site was investigated in direct shear box. For this purpose, bag samples were statically re-compacted in the laboratory to replicate closely the field condition by controlling the void ratios to be within ±5% the value of undisturbed soils. Re-compacted samples were used for direct shear tests instead of undisturbed samples, for its reproducibility and to avoid heterogeneity of the soil sample. The studied slope was recently compacted fill and thus it was thought that the re-compacted samples were adequate representatives of the material on-site.

To determine the fully saturated shear strength of the soils, slow multistage-shearing direct shear tests were carried out at normal stresses of 16, 32, 64 and 127 kPa and shearing rate of 0.05 mm/min. This rate was chosen such that no excess pore water pressure developed during shearing. Figure 13 shows the fully saturated failure envelopes in terms of effective stress. It should be noted that despite the difference in soil composition, failure envelopes of the two soils fall closely within the same range. Table 2 summarises the shear strength parameters of the materials.

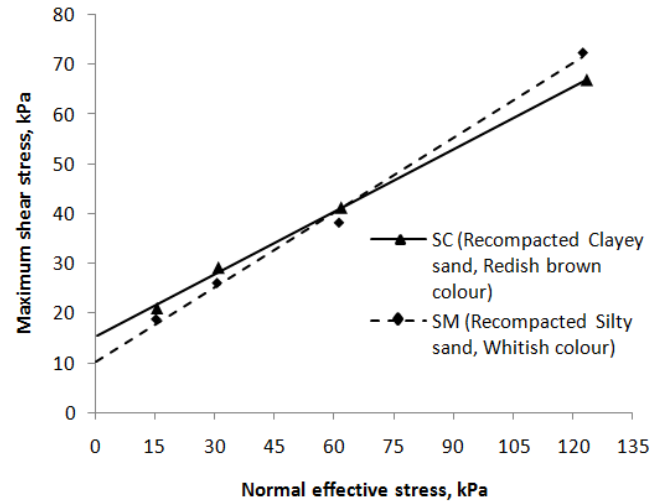


Figure 13 Fully saturated failure envelope

Table 2 Shear strength properties

Shear parameters	SC	SM
Effective cohesion, c' (kPa)	15.3	10.1
Angle of shearing resistance, ϕ'	22.7	26.7
Angle of shearing resistance with respect to suction, ϕ^{ϕ} (Peak)	38.3	32.2
Angle of shearing resistance with respect to suction, ϕ^{ϕ} (Ultimate)	7.5	18.3

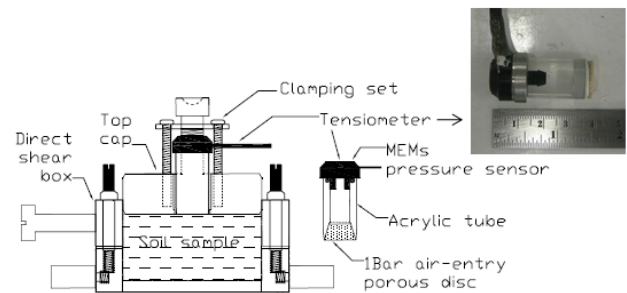


Figure 14 Suction-monitored direct shear apparatus (Jotisankasa & Mairaing, 2010)

Unsaturated shear strength was determined in the suction-monitored direct shear box as shown in Figure 14, using the test method as described by Jotisankasa & Mairaing (2010). Typical test results are shown in Figure 15 for SM soil. The samples with different initial suctions were sheared in a constant water content condition at the same normal stress of 31 kPa with shearing rate of 0.1mm/min. Evidently, the samples with higher initial suctions showed higher shear strength and tended to have the strain-softening behaviour, due to breakage of the bonding given by water menisci. At the early stages of shearing, both volume and suction of these samples decreased slightly, followed by some dilation as shear stress approached the peak value. In general, the value of suction did not change significantly during shearing in this constant-water content condition.

Figure 16 shows variation of peak and ultimate shear strength with suction for both SM and SC soils. Both materials appeared to have similar shear strengths. Unsaturated failure envelopes appeared to be nonlinear as expected for both soils, as also previously shown by many researchers (e.g., Vanapalli et al., 1996, Tepparnich & Jotisankasa, 2010). Unsaturated shear strength can be formulated using Fredlund & Rahardjo (1993) equation as shown below:

$$\tau = c' + \sigma_n \tan \phi' - u_w \tan \phi^{\phi} \tag{1}$$

where c' is effective cohesion intercept, σ_n is normal stress, ϕ' is effective angle of shearing resistance, and ϕ^b is the angle of shearing resistance with respect to suction. Note that Equation (1) assumes that pore-air pressure, u_a , equals zero. Thus, as shown in Figure 16, the value of ϕ^b varies non-linearly with suction. Nevertheless, a constant value of ϕ^b was assumed in the stability analysis software (as shown in Table 2) for convenience since the field measurement suggests that critical condition for slope involved only low value of suction (<10 kPa). The unsaturated shear strength can be reasonably modelled by assuming a constant value of ϕ^b in this case. It can also be seen in Figure 16 that the ultimate failure envelopes are very flat which suggests that the contribution of suction to shear strength becomes much less significant at a larger displacement for both materials.

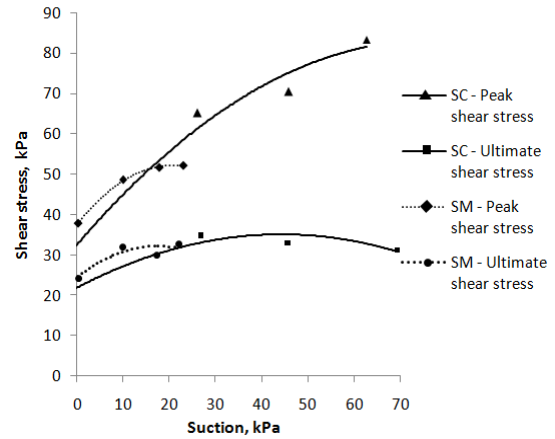


Figure 16 Unsaturated failure envelope (Shear strength vs. suction) at normal stress of 31 kPa

5. SLOPE STABILITY ANALYSIS

In order to back-calculate the value of critical pore water pressure at failure, slope stability analysis was performed based on laboratory shear strength in terms of effective stress. The General Limit Equilibrium analysis (Fredlund & Krahn, 1997) in SLOPE/W software was performed with fully specified failure surface option. The failure surface was specified as observed in the field, as shown in Figure 17. The ground water condition was specified using average value of pore water coefficient, $r_u = \frac{u_w}{\gamma H}$, while H = soil depth and γ = soil's total unit weight. The value of pore water coefficient, r_u was varied in the analysis until Factor of Safety (FS) was below 1. As shown in Figure 18, ground water condition at failure, (FS=1), corresponds to r_u value of about 0.43 for plane-strain or two-dimensional (2D) analysis.

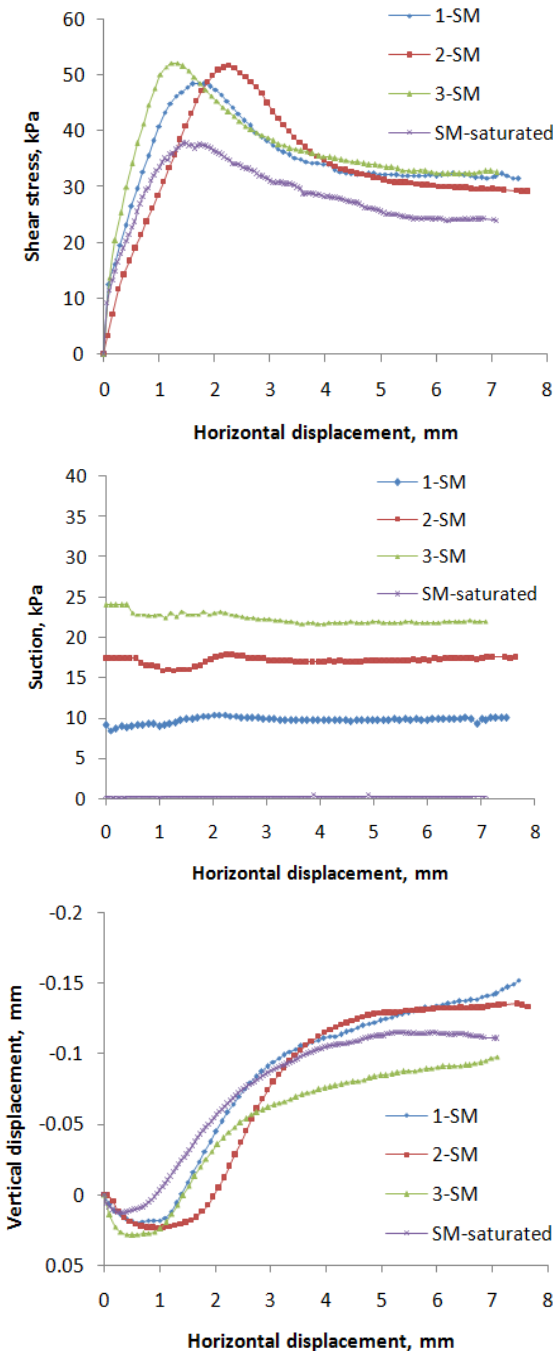


Figure 15 Typical results of suction-monitored direct shear tests at normal stress of 31 kPa for SM soil

a

b

c

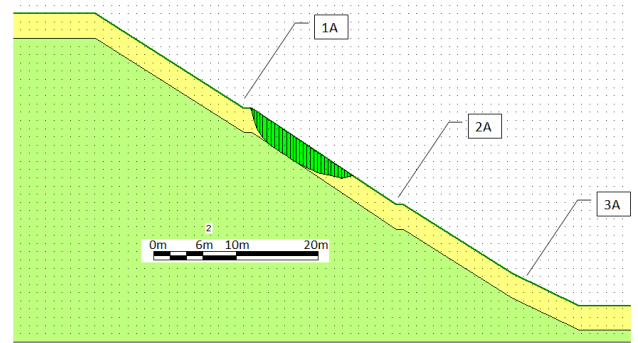


Figure 17 Stability analysis of the failed slope

Nevertheless, the actual slope failure in the field was of three-dimensional (3D) shape rather than plane-strain (2D) as assumed in conventional Limit Equilibrium analysis in SLOPE/W. In this regards, stability charts, proposed by Michalowski & Nadukuru, (2013), were used to estimate the variation of Factor of Safety with pore-water pressure coefficient, r_u , as also illustrated in Figure 18. The method was based on kinematic approach of limit equilibrium and rigid-rotation 3D mechanism. The dimension of 3D failed mass, which was expressed as B/H ratio and defined by inset in Figure 18, was estimated from field observation to be about 1.5. Generally, it has been well known that, two-dimensional (2D) stability analyses give more conservative estimates of safety factor when compared with three-dimensional (3D) analyses. As shown in Figure 18, the pore-water pressure coefficient, r_u , at failure from 3D analysis can be estimated to be about 0.57, about 30% greater, when compared with 2D analysis.

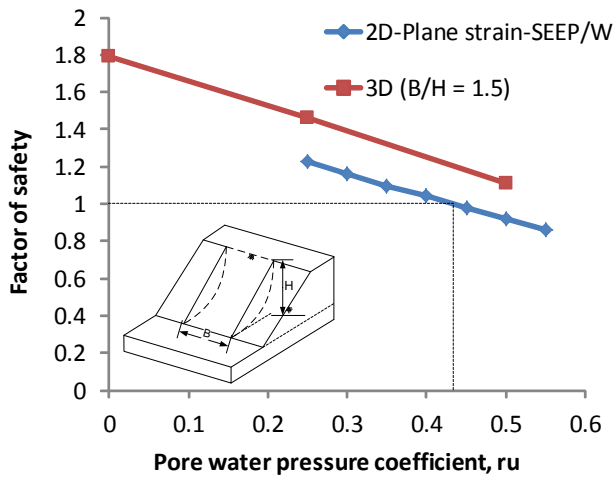


Figure 18 Variation of Factor of Safety with pore water pressure coefficient, r_u

6. SEEPAGE ANALYSIS

In this section, attempts have been made to reproduce the pore-water pressure response of slope, using 15-min rainfall as input parameters. Finite-Element seepage analysis of slope was performed using SEEP/W software, which was based on Richard's and continuity equation as shown in Equation (2):

$$\frac{\partial}{\partial x} \left[k_x \frac{\partial h}{\partial x} \right] + \frac{\partial}{\partial y} \left[k_y \frac{\partial h}{\partial y} \right] + Q = m_w \left[\frac{\partial u_w}{\partial t} \right] \quad (2)$$

where, k_x and k_y is the permeability in x and y direction respectively, h = total hydraulic head, Q = applied boundary flux or rainfall, u_w = pore water pressure, and m_w = gradient of the soil-water characteristic curve. The permeability functions used in the analysis were estimated from tested SWCCs using Jackson (1972) equation as well as saturated permeability from double-ring field infiltration tests as shown in Figure 19.

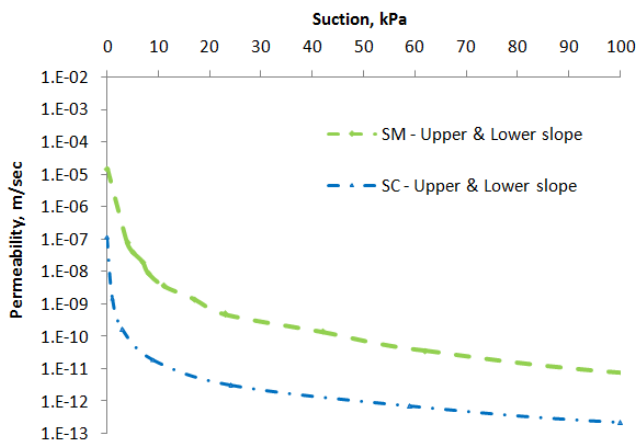


Figure 19 Permeability functions used in seepage analysis

Figure 20 shows the Finite-Element mesh and boundary conditions used in the seepage analyses. Two groups of analyses were conducted. The first group was aimed at reproducing the pore-water pressure response on 15 September 2011 obtained from field measurement. Boundary conditions and material properties were specified so that a reasonable comparison was realized between pore-water pressures from field monitoring results and SEEP/W modelling. The second group was intended to reproduce the pore

water pressure increase to failure point during 11 until 15 September 2011, during which time no field pore water pressure measurement could be obtained due to malfunction of data-loggers as explained. In this case, the modelled pore-water pressure was compared with the critical pore pressure from back analysis of slope stability instead.

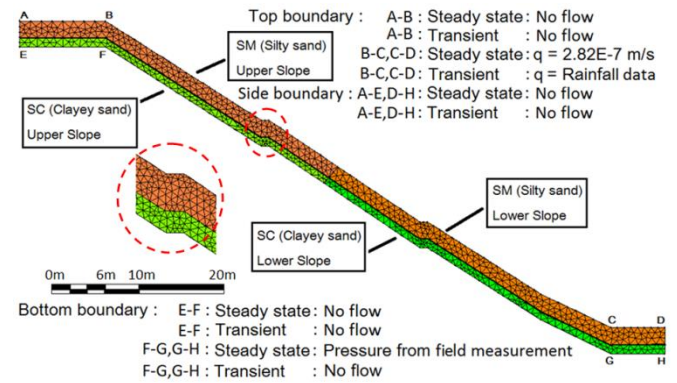


Figure 20 Finite element mesh and boundary conditions in seepage analysis

For both groups of analyses, there were two stages of simulation, namely, a) steady state (aimed at establishing the initial condition of pore water pressure in the slope) and b) transient state (to predict or reproduce the pore-water pressure response in slope due to input rainfall). The mere difference between the two groups of analysis lies in the transient state of analysis which was based on different rainfall input, q as shown in Figure 20.

The initial condition of pore-water pressure in slope was determined from steady state analysis with the flux boundary condition at the upper surface (B-C-D) specified as 2.82×10^{-7} m/s (731 mm/month), which was the average monthly rainfall during in September at the site. The boundary conditions at the base (F-G-H) in the steady state analysis were specified as fixed pressure head obtained from field tensiometer measurement. No-flow condition was assumed both at the side of top and toe boundaries (A-E & D-H). This was thought to be a reasonable assumption since there was well compacted and well paved road at the top of slope with side interceptor drain. So side flow from top of slope was believed to be minimal. For toe of slope, no-flow side boundary condition appeared reasonable for apparent condition of rock outcrop at the toe. The pore-water pressure distributions from SEEP/W analysis of initial condition were compared with field measurement as shown in Figure 21, which suggests a reasonable agreement. Figure 22 shows the initial condition of phreatic surface which indicates more water accumulated down the slope toe.

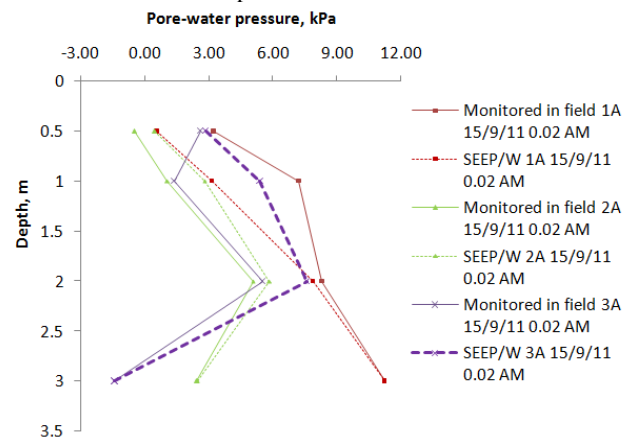


Figure 21 Pore water pressure distribution on 15 September 2014

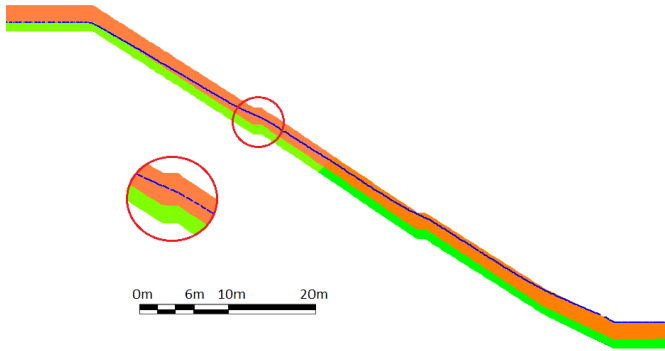


Figure 22 Initial condition of phreatic surface from steady state analysis

After initial condition had been established, transient analysis was conducted using monitored 15-min rainfall events on 15 September 2011 as upper flux boundary condition. Boundary conditions for the side and base of slope (A-E-F-G-H) for transient analysis were set to no-flow. Figures 23-25 show the variations of pore water pressure with time from field monitoring compared with SEEP/W modelling results. A satisfactory agreement was achieved between modelling and field measurement in most cases, apart from the pore water pressure at 3 m depth for Station 2A and 3A. It is expected that horizontal drain may have provided drainage path in these two locations while no-flow boundary was assumed in the analysis. It is interesting to note that a good agreement between measurement and modelling at 3m depth in Station 1A may be an indication that not enough drainage was provided by the horizontal drain due to blockage. This could perhaps explain why failure took place closer to Station 1A.

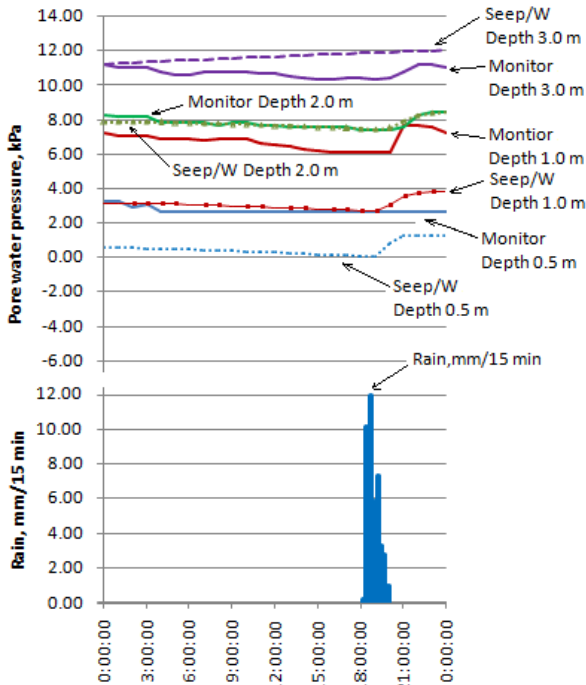


Figure 23 Pore water pressure variations with time for Station 1A from measurement and (SEEP/W) modelling (15 Sep 2011)

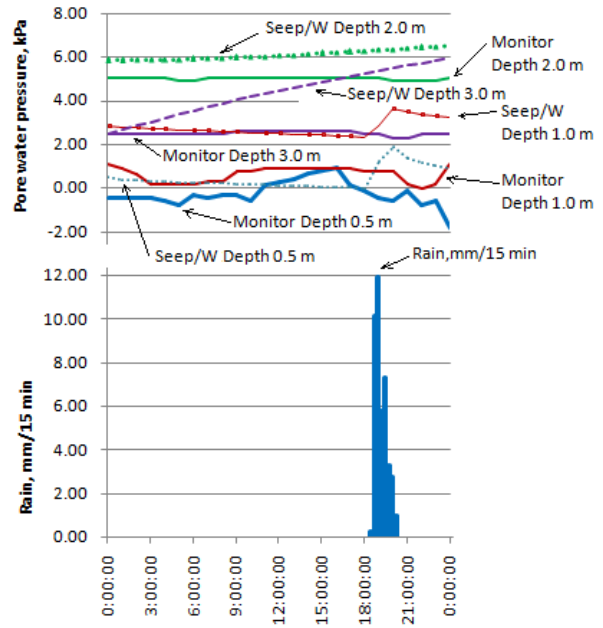


Figure 24 Pore water pressure variations with time for Station 2A from measurement and (SEEP/W) modelling

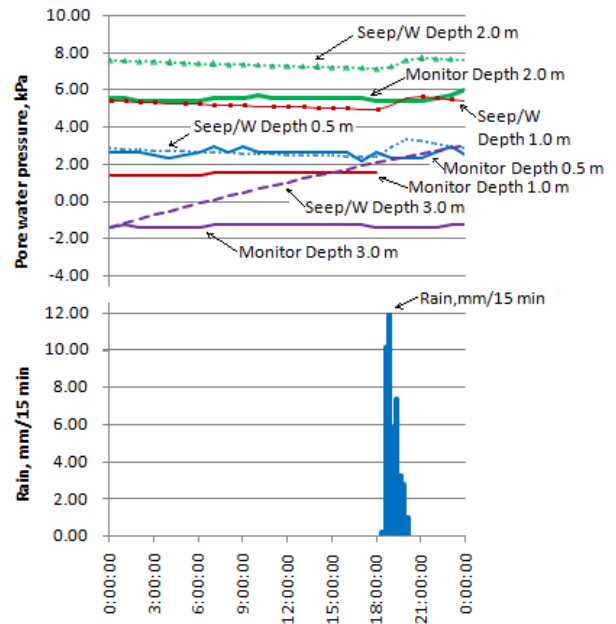


Figure 25 Pore water pressure variations with time for Station 3A from measurement and (SEEP/W) modeling

After some confidence in simulation performance had been gained, the second group of analysis was then carried out to reproduce the pore-water pressure increase to failure point and compared with the back-analysed critical pore pressure ($r_u=0.43$). The 15-min rainfall events from 11 until 15 September 2011 were taken as input flux boundary condition. Figure 26 shows the analysis results for Station 1A. Variation of simulated pore-water pressure with depth is also shown in Figure 27 compared with critical pressure distribution. Generally, the simulated pore-water pressures at shallower depth tended to converge to the critical line reasonably well. Nevertheless, the simulated pore pressures at 2m and 3m depth still had a long way to go before they converged to the critical lines.

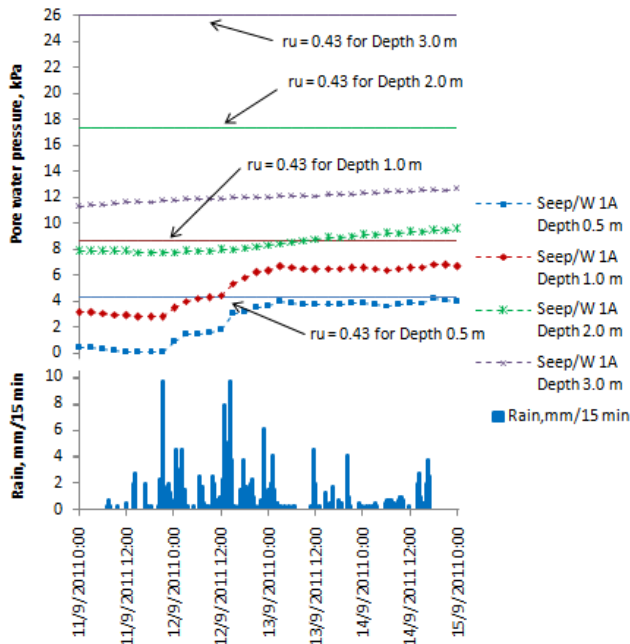


Figure 26 Prediction of pore water pressure variations during time of failure, compared with back-analyzed critical pore water pressure ($r_u=0.43$)

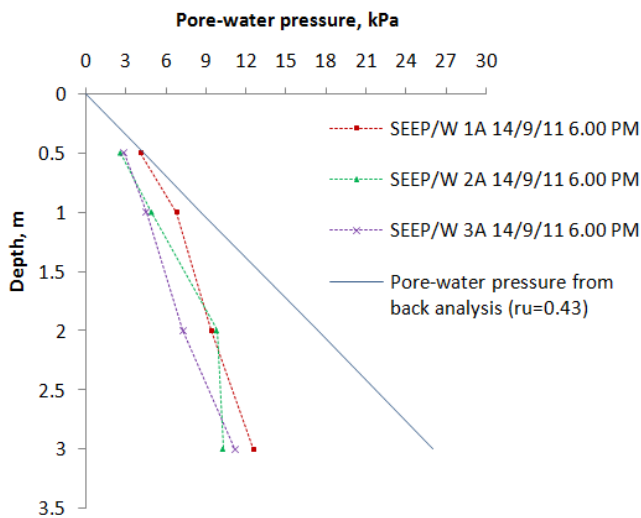


Figure 27 Predicted pore water pressure variations during time of failure, compared with back-analyzed critical pore water pressure ($r_u=0.43$)

This two-dimensional (2-D) seepage analysis thus seemed to underpredict the pore-water pressure at failure for depth greater than 2 meters. Possible explanation for this is that in reality, seepage was of three-dimensional type rather than two-dimensional. There would have been side seepages as well as runoff from areas above that contribute to greater influx of water into slope. These aspects will be investigated in the future.

7. CONCLUSION

Spatial and temporal variations of pore water pressure within slopes in response to rainfall that lead to slope failure, are one of the major uncertainties in evaluating slope stability. This paper thus presents field monitoring results of pore-water pressure and rainfall of a granitic soil slope during actual failure in September 2011. Limit

Equilibrium back analyses of stability and Finite Element seepage analyses were carried out based on saturated-unsaturated shear strength and Soil-Water Characteristic Curves (SWCC) determined in the laboratory. Some key conclusions can be drawn as follows:

- 2-D Back analysis of slope stability, for failure event in 2011 suggested that the critical pore water pressure distribution can be assigned to the r_u value of about 0.43 or $u=0.43\gamma H$. Based on 3-D stability analysis, the pore water pressure can be 30% higher when compared with the 2-D analysis.
- Field monitoring of pore water pressure using KU-tensiometers suggest that the critical zone of high seepage in slope is seasonal. The zone of high pore-water pressure also agrees well with the location of slope failure mass.
- Based on precipitation as input parameters, 2-D Finite Element seepage analysis appeared to capture general trend of pore-water pressure change reasonably well. However, it seemed to underpredict the pore-water pressure at failure especially for depth greater than 2 meters. In order to improve accuracy of the prediction, simulation of 3-D seepage, excess pore-pressure development as well as influx through run-off should be taken into account with consideration of the more complete watershed.

8. ACKNOWLEDGEMENTS

The authors are grateful to Kasetsart University Research and Development Institute (KURDI) for research grant under the project entitled “Investigation of climate change impacts on soil slopes of infrastructure in Thailand- Fiscal year 2012”. Their gratitude also goes to Chaipattana Foundation for additional financial supports and to the Department of Highways for their assistance in field study at Doi-Inthanon site. Also thankfully acknowledged is the Geotechnical Engineering Research and Development Center of Kasetsart University for providing access to the SLOPE/W & SEEP/W software used in this study. Mr. Narin Hunsachainan is also thanked for his assistance during field works.

9. REFERENCES

Buscarnera, G. & di Prisco, C. (2011) “Stability criteria for shallow unsaturated slopes” *Geotechnique Letters* 1 (4), pp 85-90.

Cascini, L., Cuomo, S., Pastor, M & Sorbino, G. (2010). “Modelling of rainfall-induced shallow landslides of the flow-type”. *Journal of Geotechnical and Geoenvironmental Engineering*. Vol. 136, No. 1

Chen, H., Lee, C.F. & Law, K.T (2004) “Causative mechanisms of rainfall-induced fill slope failures”. *Journal of Geotechnical and Geoenvironmental Engineering*, Vol. 130, No. 6

Crozier, M.J. and Eyles, R.J. (1980). “Assessing the probability of rapid mass movement”. *Proc. 3rd Aus. NZ Conf. Geomech.*, Wellington. 2: 2.47–2.51.

Evans, N.C. (1997). “The natural terrain landslide study”. *Proceedings of the annual seminar on slope engineering in Hong Kong, Rotterdam*, pp 137-144.

Fredlund, D.G. & Krahn, J. (1997) “Comparison of slope stability methods of analysis”. *Canadian Geotechnical Journal.*, Vol. 14, pp 429-439.

Fredlund, D.G. and Rahardjo, H. (1993) *Soil Mechanics for Unsaturated Soils*. John Wiley & Sons, Inc., New York.

Jackson, R.A. (1972) “On the calculation of hydraulic conductivity”. *Soil Science Society of American Proceedings*, 36, pp. 380-383

Johnson, K.A., and Sitar, N. (1990) “Hydrological conditions leading to debris-flow initiation”. *Canadian Geotechnical Journal*, Vol. 27, pp 789-801

Jotisankasa, A. and Mairaing, W. (2010) “Suction-monitored direct shear testing of residual soils from landslide-prone areas”. *Journal of Geotechnical and Geoenvironmental Engineering*, ASCE, Vol. 136, No. 3, March 1

- Jotisankasa, A. & Hunsachainan, N., Kwankeo, N., Chunrod, P. & Mancharoen, J. (2010a). "Development of a wireless landslide monitoring system". Proc. International conference on Slope. Thailand 2010. Geotechnique and Geosynthetics for Slope. Chiangmai, Thailand
- Jotisankasa, A., Tapparnich, J., Booncharoenpanich, P., Hunsachainan, N. & Sorulump, S. (2010b) "Unsaturated soil testing for slope studies". Proceedings of Int. Conference on Slope. Thailand 2010. Geotechnique and Geosynthetics for Slope. Chiangmai, Thailand
- Jotisankasa, A., Porlila, W., Sorulump, S., and Mairiang W. (2007). "Development of a low cost miniature tensiometer and its applications". Proceedings of 3rd Asian Conference on Unsaturated Soils (Unsat-Asia 2007), Nanjing, China, April 21-23
- Jotisankasa, A., Mahannopkul, K. & Sawangsuriya, A. (2014) "Evaluating slope stability with respect to pore-water pressure and suction variation with rainfall; a case study of fill granitic slope in northern Thailand", Proceedings of 6th Int. Conference on Unsaturated Soils, UNSAT 2014, Sydney Australia 2-4 July 2014, pp 1235-1240
- Kay, J.N. (1998). "Rainfall-landslide relationship update". Proceedings of the annual seminar on slope engineering in Hong Kong, Rotterdam, pp 83-86.
- Lumb, P. (1975). "Slope failures in Hong Kong". Quarterly Journal of Engineering Geology. 8: 31-65.
- Mairiang, W., Jotisankasa, A. and Sorulump, S. (2012). "Some applications of unsaturated soil mechanics in Thailand: an appropriate technology approach". Geotechnical Engineering Journal of the SEAGS & AGSSEA Vol. 43 No.1, pp. 1-11.
- Michalowski, R.L. & Nadukuru, S.S. (2013). "Three-dimensional limit analysis of slopes with pore pressure" Journal of Geotechnical and Geoenvironmental Engineering, ASCE, Vol. 139, No. 9, September 1, pp 1604-1610.
- Ng, C.W.W., Zhan, L.T., Bao, C.G., Fredlund, D.G. & Gong, B.W. (2003). "Performance of an unsaturated expansive soil slope subjected to artificial rainfall infiltration". Géotechnique, 53, 2, pp 143-157.
- Olivares, L. & Picarelli, L (2003) "Shallow flowslides triggered by intense rainfalls on natural slopes covered by loose unsaturated pyroclastic soils". Geotechnique 53(2), pp 283-287
- Sawangsuriya, A., Jotisankasa, A., Sukolrat, J., Dechasakulsom, M., Mahatumrongchai, V., Milindalekha, P. and Anuvechsirikiat, S (2013) "Comparison of Erosion Susceptibility and Slope Stability of Repaired Highway Embankment". Geo-Congress: Stability and Performance of Slopes and Embankments III Geotechnical Special Publication, Vol 231 GSP, March 2013, pp 1912-1921
- Sorbino, G. & Nicotera, M.V (2013). "Unsaturated soil mechanics in rainfall-induced flow landslides" Engineering Geology, Vol. 165, pp.105-132
- Tsaparas, I., H. Rahardjo, D.G. Toll and E.C. Leong (2003). "Infiltration Characteristics of Two Instrumented Residual Soil Slopes". Canadian Geotechnical Journal, October, Vol. 40, No.5, pp. 1012 – 1032.
- Vanapalli, S. K., D.G. Fredlund, D.E. Pufahl and A.W. Clifton. (1996). "Model for the prediction of shear strength with respect to soil suction". Canadian Geotechnical Journal, Vol. 33, pp. 379-392
- Wang, F.W., Sassa, K. & Wang, G. (2002) "Mechanism of a longrunout landslide triggered by the August 1998 heavy rainfall in Fukushima Prefecture, Japan". Engineering Geology 63, pp 169-185